ACS OMEGA

Open Access

http://pubs.acs.org/journal/acsodf

Article

Antioxidant and Anti-inflammatory Applications of *Aerva persica* Aqueous-Root Extract-Mediated Synthesis of ZnO Nanoparticles

Kaneez Fatima, Mohammad Asif, Umar Farooq,* Sadaf Jamal Gilani, May Nasser Bin Jumah, and Mohammed Muqtader Ahmed

Cite This: *ACS Omega* 2024, 9, 15882−15892

Read Online

ACCESS | Metrics & More | Article Recommendations

ABSTRACT: In the present study, ZnO nanoparticles were synthesized by using aqueous extracts of *Aerva persica* roots. Characterization of as-prepared ZnO nanoparticles was carried out using different techniques, including powder X-ray diffraction (XRD), UV−vis diffuse reflectance spectroscopy (DRS), Fourier transform infrared (FTIR) spectroscopy, field emission scanning electron microscopy (FESEM), transmission electron microscopy (TEM) and BET surface area analysis. Morphological analysis confirmed the small, aggregated flake-shaped morphology of as-synthesized ZnO nanostructures. The as-prepared ZnO nanoparticles were analyzed for their potential application as anti-inflammatory (using in vivo inhibition of carrageenan induced paw edema) and antioxidant (using in vitro radical scavenging activity) agents. The ZnO nanoparticles were found to have a potent antioxidant and anti-inflammatory activity comparable to that of standard ascorbic acid (antioxidant) and indomethacin (anti-inflammatory drug). Therefore, due to their ecofriendly synthesis, nontoxicity, and biocompatible nature, zinc oxide nanoparticles synthesized successfully from roots extract of the plant *Aerva persica* with potent efficiencies can be utilized for different biomedical applications.

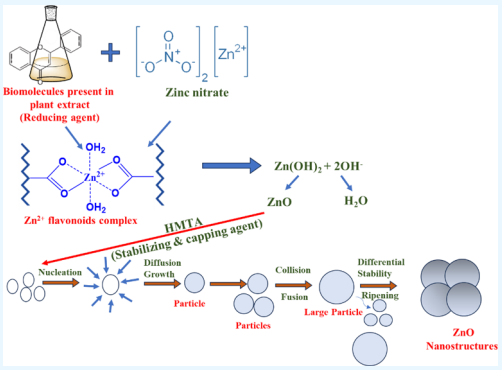

1. INTRODUCTION

Nanotechnology is now regarded as a proven cutting-edge technology with numerous applications in the food processing, mechanical, chemical, and pharmaceutical industries. Nanotechnology can also be used in optics, computing, power production, drug delivery, and environmental sciences.[1] Since the emergence of nanotechnology, numerous nanoscale devices have been created utilizing several techniques, including physical, chemical, and environmentally friendly ways. However, the green synthesis route for nanomaterials is found to be a simple versatile route that can be easily engineered.[2] There are certain limitations of conventional nanoparticle synthesis methods (which include most physical and chemical routes) including prolonged processing times, high reaction temperature, high costs, and particularly the utilization of toxic compounds. Due to these limitations, most of the relevant research has focused on environmental benign and rapid synthesis routes for nanoparticle synthesis.[3−8] Green synthesis of NPs, notably using plant extracts, is an emerging trend in green chemistry that is regarded as simple, economical, and safe.[9−12] Several plant extract-mediated syntheses of different metal and metal oxide-based materials have been reported for application in different fields.[13−15] Among different metal oxides, ZnO nanoparticles are intriguing inorganic materials that offer innumerable benefits involving various fields such as energy conservation, electronics, textiles, cosmetics, healthcare, semiconductors, chemical sensing, and catalysis. Interestingly, these nanoparticles are biocompatible, safe to employ, and have tremendous biological functions.[16−18] As an essential trace element, zinc is widely present in all biological tissues, including the brain, muscle, bone, and skin, among others. Being the primary component of numerous enzyme systems, zinc participates in the body's metabolism and plays key roles in the production of proteins and nucleic acids, hematopoiesis, and neurogenesis.[19] Because of its extremely small particle size, nanosized ZnO enables zinc to be absorbed by the body with greater efficiency. Furthermore, the US Food and Drug Administration (FDA) has classified ZnO as a "GRAS" (generally regarded as safe) chemical.[20] When compared to other metal oxide nanoparticles, ZnO NPs have outstanding biomedical applications such as anticancer, drug delivery, diabetic treatment, wound healing, anti-inflammation, anti-

Received: October 17, 2023
Revised: March 13, 2024
Accepted: March 18, 2024
Published: March 29, 2024

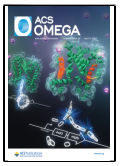

Scheme 1. Schematic Representation of Possible Reaction Mechanism Involved in Synthesis of ZnO Nanoparticles

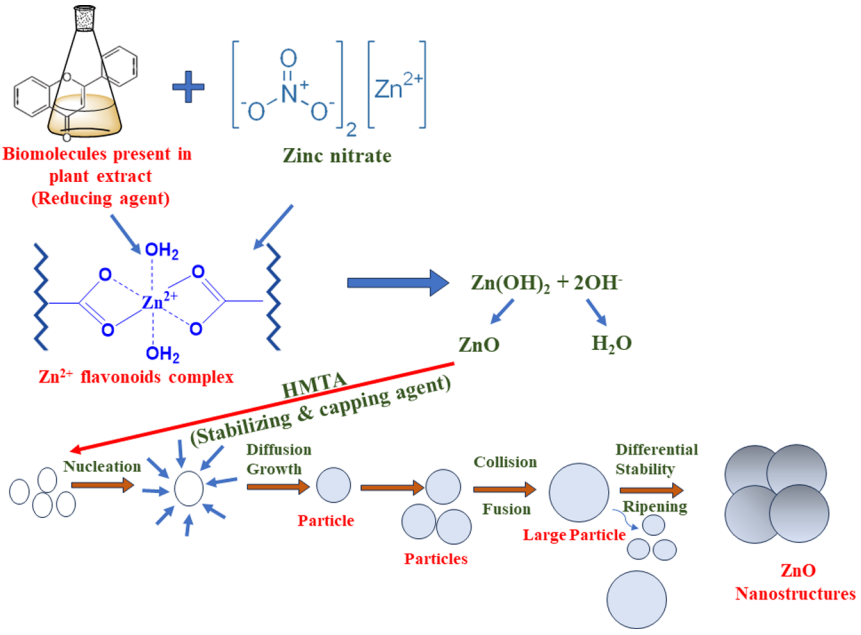

bacterial, and antioxidant.[21−24] Based on earlier reports different plant-extract-mediated methodologies have been developed for the synthesis of ZnO nanoparticles using extracts from different components like leaves, bark, shoots, and roots of a plant.[19] Several researchers have employed these plant-extract-mediated synthesized ZnO nanoparticles as improved antioxidant, antiinflammation, and anticancer agents.[25−29]

For normal metabolism, free radicals and antioxidants are present in balanced concentration. However, excessive creation of free radicals is linked to oxidative damage as well as several chronic disorders, including diabetes, inflammation, and cancer. Consuming antioxidants can help to protect the body against the harm that is caused by free radicals. Due to their toxicity, synthetic antioxidants are no longer widely used. For this reason, scientists are now investigating natural antioxidants.[30,31]

Inflammation is a defense process against a variety of threats, such as pathogens, chemicals, immune responses, poisons, hypoxia, and damaged tissues.[32] The inflammatory response is characterized by the activation of white blood cells as well as the release of chemicals produced by the immune system. These chemicals include pro-inflammatory cytokines such as IL-1, IL-6, IL-12, IL-18, TNF, INF- γ, and granulocyte-macrophage colony (GMS-CF) stimulating factor. The nuclear factor-k beta (NF-kb) transcription factor is responsible for regulating the expression of several genes, including those that code for pro-inflammatory cytokines, adhesion molecules, chemokines, growth factors, and inducible enzymes such as COX-2 and iNOS, which are known to stimulate the production of pro-inflammatory mediators.[33]

Nano-dimensional ZnO with a wide range of properties and applications can be created using a variety of methods (chemical, physical, and biosynthesis). Plant-mediated preparation of ZnO nanoparticles has been reported many times in the past; however, there is a lack of literature on their various biological properties, such as antioxidant and anti-inflammatory activities.

In the current study, zinc oxide nanoparticles were prepared via a green method involving an aqueous root extract of the *Aerva persica* plant. The plant *Aerva persica* has been shown to have hypoglycaemic, antioxidant, antimalarial, anthelmintic, analgesic, antivenin, and antikidney-disease and rheumatism properties. *A. persica* also demonstrated antiviral, antiplasmodial, and antidiabetic activities. Considering the already established biological activities of *Aerva persica*, we have tried to employ different phytochemicals present in the roots of *Aerva persica* for the synthesis of ZnO NPs. The phytochemical flavonoids, which are responsible for the ZnO nanoparticles synthesis, primarily act as reducing and stabilizing agents.[34−36] To the best of our knowledge, no report on the green synthesis of ZnO-NPs using *Aerva persica* aqueous root extract is available. The current study investigates the green synthesis of ZnO-NPs, their characterization, and the investigation of in vitro antioxidant activity.

2. EXPERIMENTAL SECTION

2.1. Materials and Methods. For synthesis of ZnO analytical grade zinc nitrate, ($Zn(NO_3)_2.2H_2O$, Merck, 13778-30-8), Sodium hydroxide (NaOH, Merck, 1310-73-2), Hexamethylenetetramine (HMTA), ($C_6H_{12}N_4$, SRL, 100-97-0), Ethanol (C_2H_5OH, SRL, 64-17-5), and double distilled water were employed. In addition, L-Ascorbic acid ($C_6H_8O_6$, SRL, 50-81-7), 2, 2′-azino-bis-(3- ethylbenzothiazoline-6-sulfonic acid) (ABTS) ($C_{18}H_{24}N_6O_6S_4$, 30931-67-0), 2,2′-diphenyl-1-picrylhydrazyl (DPPH) ($C_{18}H_{12}N_5O_6$, 1898-66-4), Hydrogen peroxide, (H_2O_2, Sigma Aldrich, 7722-84-1), Indomethacin (indocrom-50) ($C_{19}H_{16}ClNO_4$, 53-86-1), (Orion life science, Ahmedabad) was purchased from local drug store. Carageenan, (CDH fine chemicals, New Delhi, 9000-07-1). In all the studies, the compounds were used in their unpurified, as-bought form without any additional pretreatment.

2.2. Plant Collection and Extraction. *Aerva persica* was identified, and its roots were collected from the local area of Jodhpur, Rajasthan. The plant species were identified and authenticated by the Botany department of Biwal Medchem

https://doi.org/10.1021/acsomega.3c08143
ACS Omega 2024, 9, 15882−15892

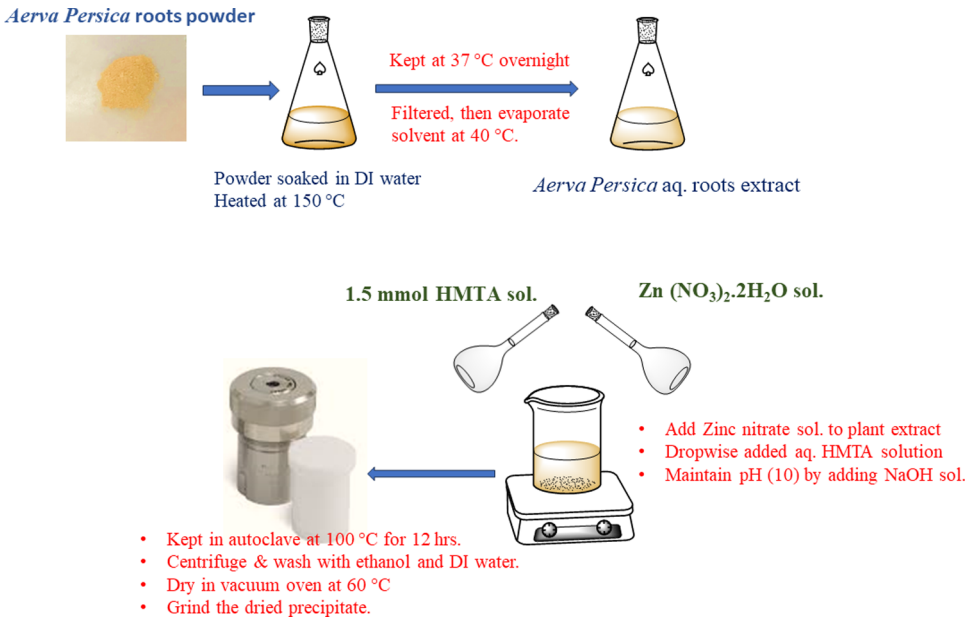

Figure 1. Schematic representation of reaction setup used, and reaction steps involved in synthesis of ZnO NPs using *A. persica* root extract.

and Research Laboratory Pvt. Ltd., Jaipur, Rajasthan with Reference no: BMRL/PA/2021-16. The plant extract was acquired by using a previously reported method.[37] For the preparation of extracts, the plant material was pulverized to a fine powder using an electric grinder. Before heating to 150 °C, 50 g of plant powder was soaked for 20 min in 500 mL of double-distilled water. To optimize extraction, the soaked powder was maintained in an incubator at 37 °C overnight. After the extract was filtered through Whatman filter paper no. 1823, the solvent was evaporated in a rotatory evaporator at 40 °C. The left-out plant extract was kept at 4 °C in the refrigerator.

2.3. Synthesis of ZnO Nanoparticles. The zinc oxide nanoparticles were synthesized by using a green, cost-effective hydrothermal route. Briefly, 3.0 g of Zn $(NO_3)_2{\cdot}2H_2O$ was dissolved in 5 mL of double distilled water. In another beaker, 5 mL of plant extract was heated at 50 °C for 10 min, and a previously prepared aqueous solution of Zinc nitrate dihydrate was added dropwise into it. Afterward, 1.5 mmol (0.21 g) of HMTA was poured into the above suspension. The pH of the solution (pH 10) was maintained by using 0.06 M (10 mL) NaOH solution, and the solution was kept at a magnetic stirrer for 30 min at 800 rpm to obtain a turbid suspension. After that, the suspension was placed inside an autoclave lined with Teflon and heated to a temperature of 100 °C for a period of twelve hours. The mixture was coolled and centrifuged once it reached room temperature, and the resulting precipitate was washed with distilled water and ethanol. Lastly, the product was dried at 60 °C to produce ZnO nanoparticles (with approximately 82% yield). The probable mechanistic steps involved during the synthesis of ZnO NPs are depicted in scheme 1. The influence of plant extract on the production of ZnO nanoparticles was investigated by changing the ratio of plant extract to zinc nitrate (v/w) and determining the resulting ZnO nanoparticles yield which is calculated by using eq 1:[38]

$$\text{Yield}\ (\%) = \left(\frac{\text{Experimental weight of ZnO}}{\text{theoretical weight of ZnO}}\right) \times 100 \quad (1)$$

The reaction setup and reaction steps used during the synthesis of ZnO nanoparticles are shown in Figure 1.

2.4. Characterizations. Powder X-ray diffraction analysis with a D/Max 2500 diffractometer set at a scan rate of 5°/min in the 2θ range 20−80° with Cu Kα radiation (1.54 Å) was used to investigate the crystal structure, purity, crystallinity, and phase of the as-prepared nanoparticles. Nanoparticles were tested for their optical properties using a PerkinElmer 365 double-beam UV−vis diffuse reflectance spectrophotometer (DRS) in the wavelength range 200−800 nm. Attenuated Total Reflection-Fourier Transform Infrared (FTIR) Spectroscopy was carried out, and spectra were recorded at FTIR spectrophotometer model IR affinity 1. To analyze the morphology, chemical composition, and elemental distribution, field emission scanning electron microscopy (FESEM) and energy dispersive X-ray studies were performed using a Zeiss Corporation Gemini SEM-500 apparatus at an accelerating voltage of 20 kV. For FESEM investigation, to prevent a surface charging effect, a dry sample was placed on ultrathin gold-coated carbon tape. Using transmission electron microscopy (TEM) with a FEI Tecnai G2 20 instrument at a 200 kV acceleration voltage, the size and morphology of as-synthesized nanoparticles were determined. Powdered nanoparticles were ultrasonically dispersed in ethanol for 30 min before being drop-cast onto carbon-coated copper grids for TEM/HRTEM imaging. The surface area and pore size of as-synthesized nanoparticles were measured using a Brunauer−Emmett−Teller (BET) (Novatouch LX4, Quantachrome Instruments Limited), surface area analyzer at liquid nitrogen temperature (77 K). Before conducting the analysis, surface contaminants and moisture were removed by carrying out an overnight vacuum degassing process. This was accomplished by inserting 0.08 g of sample in the sample cell and heating it to 120 °C. Using the multipoint BET equation (eq 2), the surface area of the as-synthesized nanoparticles was estimated.

$$\frac{P/P_0}{V[1 - P/P_0]} = \frac{c - 1}{V_m c}\left(\frac{P}{P_0}\right) + 1/V_m c \quad (2)$$

https://doi.org/10.1021/acsomega.3c08143
ACS Omega 2024, 9, 15882−15892

where P and P_0 represent the equilibrium and saturation pressure of adsorbates, respectively, V is the volume of the adsorbate gas, V_m represents the volume of gas adsorbed in monolayer adsorption, and c represents the BET constant.

2.5. In Vitro Antioxidant Activity. *2.5.1. DPPH Radical Scavenging Activity.* ZnO NPs were evaluated for their 2,2′-diphenyl-1-picrylhydrazyl (DPPH) radical scavenging activity to evaluate its antioxidant properties. During analysis, ascorbic acid was employed as a standard antioxidant agent. In methanol, a 0.1 mM DPPH solution was prepared, and 3 mL of this solution was mixed with 1 mL of ascorbic acid. Similarly, ZnO NPs at various concentrations (100, 250, and 500 μg/mL) were mixed in 3 mL of methanol solution of DPPH. After mixing the reaction mixture was sonicated and placed in the dark for 30 min. At 517 nm, the absorbance of the reaction mixture was measured. The percentage of DPPH scavenging activity was evaluated using eq 3:[39,40]

$$\text{Percentage of inhibition } \% = \frac{(A_c - A_t)}{(A_c)} \times 100 \quad (3)$$

A_c = absorbance of control; A_t = absorbance of test sample.

2.5.2. H_2O_2 Radical Scavenging Assay. ZnO NPs were evaluated for their H_2O_2 radical scavenging activity using ascorbic acid as a reference standard; 4 mM of H_2O_2 in a 0.6 mL of phosphate buffer (pH 7.4) was added to 0.5 mL of known concentration of ascorbic acid, as well as to the various concentrations of ZnO NFs (100, 250, 500 μg/mL in phosphate buffer). The reaction mixtures were kept for 10 min. After 10 min, the absorbance of the reaction mixture was taken at 230 nm using a blank solution (phosphate buffer and hydrogen peroxide free). The absorbance was taken in triplicate.[41] Percentage inhibition was calculated by using eq 3.

2.5.3. 2, 2′- Azino-bis-3-ethylbenzothiazoline-6-sulfonic Acid (ABTS) Radical Scavenging Assay. The ABTS radical was prepared as per González-Palma et al., 2016. The reaction mixture consisted of 0.07 mL of ZnO NPs and ascorbic acid solution at various concentrations (100, 250, 500 μg/mL) 0 and 3 mL of prepared ABTS radical. The reaction mixtures were incubated for 6 min. Afterward, the absorbance was measured at 734 nm. Percentage Inhibition of ABTS scavenging activity was calculated as formula given in eq 3 given above.[42]

2.6. In Vivo Anti-Inflammatory Activity. *2.6.1. Experimental Animals.* Wistar albino rats, aged 6−8 weeks, 170−200 g, were procured and housed in the animal house facility of Bilwal Medchem and Research Laboratory Pvt. Ltd., Reengua Industrial area (RIICO), Sikar, Rajasthan. They were given a standard diet and water ad libitum. The temperature was maintained at 22 °C (±3 °C), humidity was maintained at 40−60%, and artificial lighting was maintained as a 12 h light and dark sequence. The experimental protocol was approved as per the Committee for the Purpose of Control and Supervision of Experiments on Animals (CPCSEA) and Institutional Animals Ethics Committee (IAEC) of Bilwal Medchem and Research Laboratory Pvt. Ltd. (Reg No-2005/PO/RcBT/18/CPCSEA).

2.6.2. Inhibition of Carrageenan Induced Paw Edema. There were three groups created from the Wistar albino rats. Group I served as the negative control and received 0.1 mL of carrageenan suspension in the subplantar region of the right hind paw. Group II served as the standard and was administered with indomethacin (50 mg/kg) and carrageenan (0.1 mL). Group III served as the test group and received ZnO NPs (36.5 mg/kg) and 0.1 mL of carrageenan. The volume displacement (VD) of mercury in mL was measured using a mercury plethysmometer at 0, 1, and 2 h of drug administration.[43,44] The percent inhibition of edema was calculated as in eq 4:

$$\text{Percentage of inhibition } \% = \frac{(\text{VD in untreated group} - \text{VD in treated group})}{(\text{VD in untreated group})} \times 100 \quad (4)$$

3. RESULTS AND DISCUSSION

3.1. X-ray Diffraction Analysis. For the examination of structural properties, a powder X-ray diffractometer was employed with a step size of 0.05° and a step time of 1 s, from (2θ) 10° to 80°. To get correct lattice constants, the $K_{\alpha 1}$ reflections were used. Figure 2 shows the XRD diffraction pattern of as-synthesized *Aerva persica*-mediated ZnO nanoparticles, which was well-matched with JCPDS card no. 80−0075 for zinc oxide. The significant diffraction peaks observed at 2θ values of 31.6, 34.4, 36.1, 47.5, 56.4, 62.6, 66.2, 67.8, 69.04, 72.4, 76.9 corresponds to the reflections from (100), (002), (101), (102), (110), (103), (200), (112), (201), (004) and (202) crystal planes of the hexagonal wurtzite zinc oxide structure. No impure peaks corresponding to secondary phases were identified, confirming the phase purity and monocrystallinity of as-synthesized ZnO nanoparticles, whereas the intense diffraction peaks of the as-prepared *Aerva persica*-mediated ZnO nanoparticles indicate their high crystallinity. By employing Debye−Scherrer's formula eq 5, the average crystallite size was calculated.[45]

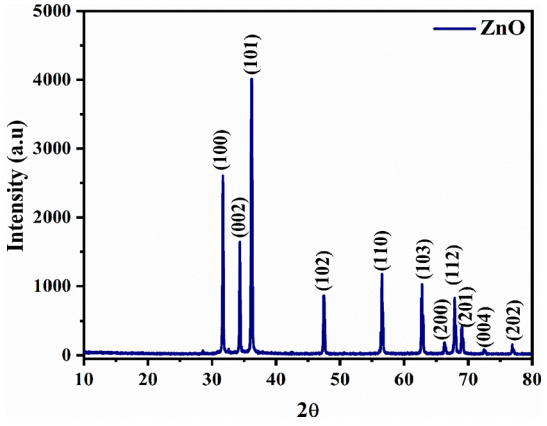

Figure 2. Powder X-ray diffraction pattern of as-synthesized *Aerva persica* mediated ZnO nanoparticles.

$$D = K\lambda/\beta\cos\theta \quad (5)$$

where D represents crystallite size, K denotes Scherrer's constant (0.94), λ denotes wavelength of incident X-rays, β is the full width at half-maximum (fwhm) value of diffraction peaks, and θ indicates diffraction angle. The as-calculated average crystallite size of the as-synthesized *Aerva persica*-mediated ZnO nanoparticles was found to be 23.84 nm. The lattice constants of as-synthesized *Aerva persica* ZnO nanoparticles were determined by using the below-mentioned eq 6.[46]

https://doi.org/10.1021/acsomega.3c08143
ACS Omega 2024, 9, 15882−15892

$$\frac{1}{d^2} = \frac{4(h^2 + hk + k^2)}{3a^2} + \frac{l^2}{c^2} \quad (6)$$

where d represents lattice spacing which was determined by employing Bragg's equation, i.e., $2d \sin\theta = n\lambda$, and the volume of the unit cell was also evaluated using relation $V = 0.866\ a^2$. The values of as-calculated lattice constants and cell volume were found to be $a = b = 3.176$ Å, $c = 5.281$ Å, and $V = 45.66$ Å respectively.

3.2. UV−Vis DRS Studies. As-prepared *Aerva persica*-mediated ZnO nanoparticles were examined by employing diffuse reflectance UV−vis reflectance spectroscopy to investigate the optical properties. Figure 3a displays the

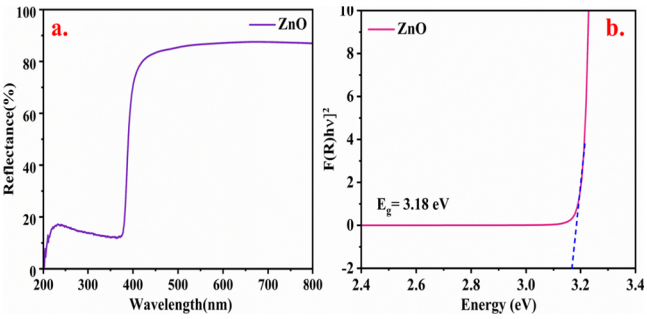

Figure 3. (a) UV−vis reflectance spectra (b) Kubelka−Munk plot for band gap of as-synthesized *Aerva persica* mediated ZnO nanoparticles.

reflectance plot of as-synthesized ZnO nanoparticles attained from DRS analysis, and Figure 3b displays the Kubelka−Munk plot which is the plot of photon energy ($h\upsilon$) versus $[F(R)\ h\upsilon]^2$ on x and y-axis respectively. The band gap is calculated by the linear extrapolation of the Kubelka−Munk plot. Figure 3a shows that the optical reflectance spectra reveal the absorption peak around ∼400 nm, which is consistent with reported studies.[47] By employing the Kubelka−Munk equation, the optical band gap is calculated which is expressed in eq 7.

$$F(R) = \alpha/s = (1 - R^2)/2R \quad (7)$$

where $F(R)$ represents the Kubelka−Munk function, α is the absorption coefficient, s denotes the scattering factor, and R denotes the reflectance of a material. The estimated band gap value for as-synthesized *Aerva persica*-mediated ZnO nanoparticles agrees with recently reported studies and was found to be 3.18 eV.[48]

3.3. Fourier Transform Infrared Spectroscopy. As illustrated in Figure 4, FTIR spectroscopy was done in the range 500−4000 cm^{-1} to characterize the functional groups in the aqueous extract of *Aerva persica* roots and zinc oxide nanoparticles. Figure 4a displays the FTIR spectra of aqueous extract of *Aerva persica* roots where the strong adsorption band around 2882, 2185, 1856, 1683, 1382, and 1106 cm^{-1} corresponds to O−H/N−H/C−H, C═O and C−Cl/C−S stretching/bending vibrations respectively indicate the presence of amino acids, alkenes, nitrates, ethers, organic halogen compounds and carbohydrates in the root extract of *Aerva persica*. The presence of carbonyl functional groups is indicated by the bands appearing at around 2882 cm^{-1} (C−H stretching), 1683 cm^{-1} (C═O stretching), and 1382 cm^{-1} (C−CO−C stretching). The very strong adsorption band around 3571, 3260, and 2882 cm^{-1} is due to the presence of bonded N−H/C−H/O−H stretching of amines and amides. Figure 4b displays the FTIR spectra of *Aerva persica* root

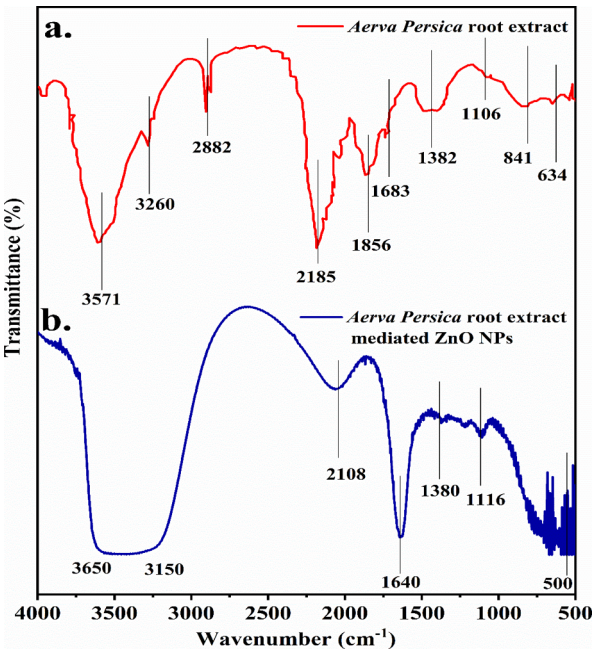

Figure 4. FTIR spectra of (a) *Aerva persica* root extract and (b) as-synthesized *Aerva persica*-mediated ZnO nanoparticles.

extract-mediated ZnO NPs. The peak around 500 cm^{-1} was attributed to bonding vibrations between zinc and oxygen M−O bond.[49] The peak noticed at 1640 cm^{-1} is due to the water molecule's O−H bending vibration. The O−H stretching vibrations of water molecules and the N−H stretching vibrations of amines and amides[50] are responsible for the extended band from 3150 to 3650 cm^{-1}. The peak around 2108 cm^{-1} is attributable to the C═C stretching vibration.[51] The C═O stretching vibrations of carboxylic acid are situated at 1380 and 1116 cm^{-1}[52] respectively. The results obtained from FTIR analysis confirm the presence of biomolecules including terpenoids, flavonoids, tannins, and proteins that may be present in as-synthesized *Aerva persica*-mediated ZnO nanoparticles.

3.4. Field Emission Scanning Electron Microscopic Studies. The morphological analysis of as-synthesized *Aerva persica*-mediated ZnO nanoparticles was done by the SEM technique. Figure 5a displays the SEM micrograph of as-synthesized ZnO nanoparticles at 5 μm scale which shows tiny flakes-like particles that are highly agglomerated to form rough and coarse morphology of nanoparticles. Figure 5b displays the high-resolution micrograph which shows flakes-like particles that overlap, which results in the growth of nanoparticles.

3.5. Energy Dispersive X-ray Analysis. The elemental composition of as-synthesized *Aerva persica*-mediated ZnO nanoparticles was investigated by employing EDX analysis. Figure 6 displays the EDX spectra of as-synthesized *Aerva persica*-mediated ZnO nanoparticles, which exhibited strong EDX peaks for oxygen (O) and Zinc (Zn) elements. The peak observed at 0.5 keV corresponds to the K-shell of oxygen and peaks at 1.0 and 8.6 keV corresponds to zinc. The inset of Figure 6 displays that the atomic weight of oxygen is found to be 61.97%, while its weight present is 28.50%. Moreover, the atomic weight of zinc is found to be 38.03%, and its weight present is 71.50%. There are some other minor constituents present in the as-synthesized nanoparticles due to the presence of a plant extract.

https://doi.org/10.1021/acsomega.3c08143
ACS Omega 2024, 9, 15882−15892

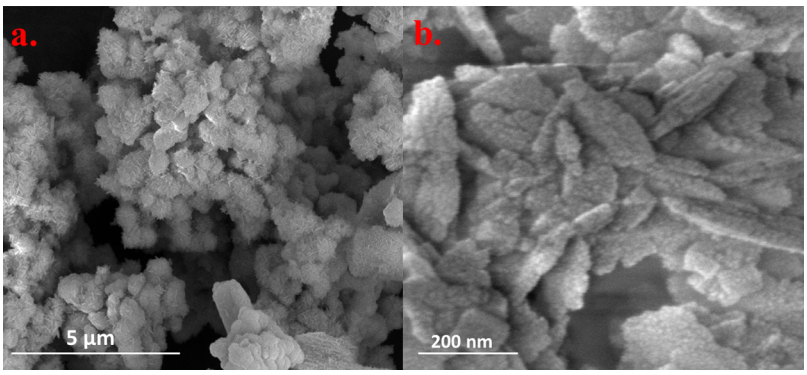

Figure 5. FESEM micrographs at two different resolutions (a) 5 μm and (b) 200 nm of as-synthesized *Aerva persica*-mediated ZnO nanoparticles.

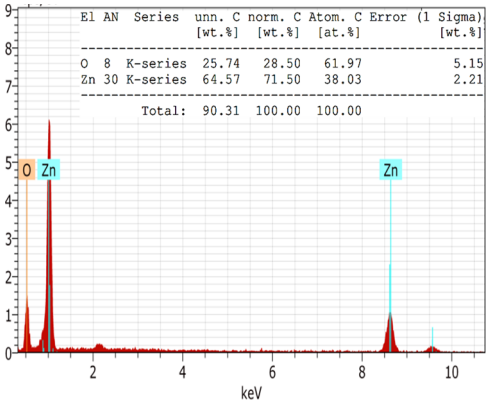

Figure 6. EDX spectra of as-synthesized *Aerva persica*-mediated ZnO nanoparticles.

3.6. Transmission Electron Microscopic Studies. To further investigate the shape and size of as-syntchesized *Aerva persica*-mediated ZnO nanoparticles, TEM analysis was carried out. Figure 7a,b shows the TEM micrographs of as-synthesized ZnO nanoparticles at two different resolutions. It could be seen that as-synthesized ZnO nanoparticles have rough morphology with no defined shape. It can be observed that the edges of the ZnO nanoparticles were not smooth. Using Image J software size distribution of as prepared sample was determined as shown in the size distribution histogram in Figure 7c. The average particle size calculated from the TEM micrograph is shown in Figure 7b using ImageJ software, which was found to be ~45 nm.

3.7. BET Surface Area Studies. The surface area is the most important parameter to be investigated before analyzing the different activities of nanoparticles. The high surface area of metal oxide-based nanoparticles enhances their properties, resulting in better efficiency in different applications. It is estimated that better results for biological activities will be

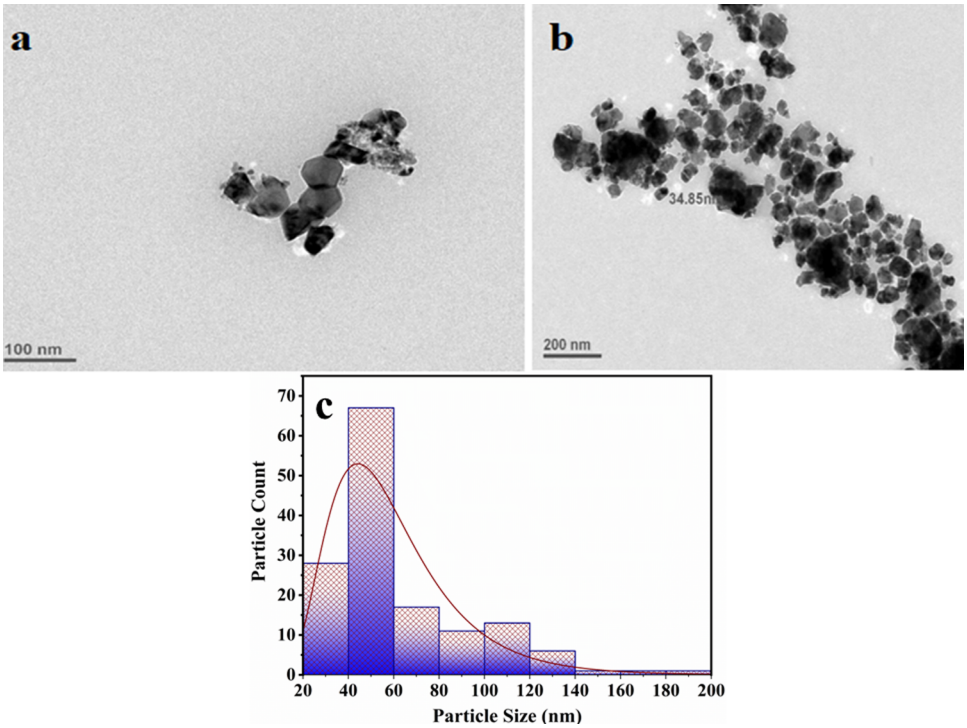

Figure 7. TEM micrographs at two different resolutions (a) 100 and (b) 200 nm and (c) particle size histogram of as-synthesized *Aerva persica* mediated ZnO nanoparticles.

https://doi.org/10.1021/acsomega.3c08143
ACS Omega 2024, 9, 15882−15892

achieved through synthesizing nanomaterials with a high surface area. By employing the multipoint BET method, the surface area of as-synthesized *Aerva persica*-mediated ZnO nanoparticles was determined through nitrogen adsorption−desorption measurements. Figure 8 shows the nitrogen

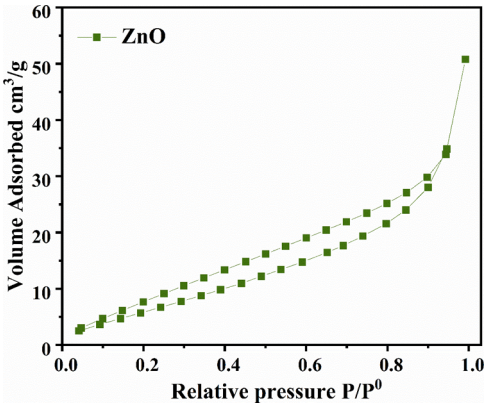

Figure 8. BET isotherm of as-synthesized *Aerva persica* mediated ZnO nanoparticles.

adsorption−desorption isotherm of as-prepared *Aerva persica*-mediated ZnO nanoparticles, which followed a type III BET isotherm pattern and an H3-type-hysteresis loop.[53] The surface area of as-synthesized ZnO nanoparticles was found to be 43 m^2/g. The comparative analysis of the BET surface area of ZnO nanoparticles synthesized by using *Aerva persica* plant extract with previously reported literature is given in Table 1.

Table 1. Comparative BET Surface Area of the As-Synthesized ZnO Nanoparticles with the Previously Reported Literature

sample	synthesis approach	surface area (m^2/g)	ref
ZnO nanoparticles	*Aerva persica* mediated	43	this work
ZnO nanoparticles	sol−gel	10.52	54
ZnO nanoparticles	solid-state pyrolytic	12−30	55

3.8. In Vitro Antioxidant Activities. In the present study, biosynthesis of ZnO NPs was carried out by *Aerva persica* root extract, and its antioxidant activity was evaluated using different radical scavenging activities.

3.8.1. DPPH Radial Scavenging Activity. DPPH free radical scavenging activity is widely used as an in vitro model for the evaluation of antioxidant activity. An antioxidant donates its hydrogen which leads to reduction of DPPH solution to diphenylpicyl hydrazine.[56] Percent of DPPH radical scavenging activity of ZnO NPs and ascorbic acid were evaluated using the above-mentioned approach, and the obtained results are presented in table 2. DPPH scavenging activity of ZnO NPs was found to be lower than ascorbic acid at 100 μg/ml ($p < 0.0001$). However, DPPH radical scavenging activity of ZnO NPs is higher as compared to ascorbic acid at 250 μg/ml, while as no significant difference was observed in 500 μg/ml, which signifies that the DPPH radical scavenging activity of ZnO NPs was comparable to that of standard ascorbic acid. In addition to ZnO NPs antioxidant activity of root extract used to synthesize nanoparticles was analyzed and no significant activity was observed which confirms that reduction of DPPH is solely carried out by ZnO nanoparticles.

3.8.2. H_2O_2 Scavenging Activity. Hydrogen peroxide is a mild oxidizing agent that directly inactivates few enzymes by oxidizing their crucial thiol (−SH) groups. It may swiftly traverse cell membranes; once within the cell, it may combine with Fe^{2+} and perhaps Cu^{2+} ions to produce hydroxyl radicals, which may be the source of many of its harmful effects. Although it is not harmful by itself,[57] however, can be transformed to much more dangerous radicals such as OH by the Fenton reaction or hypochlorous acid by the myeloperoxidase enzyme.[58] Hence, the elimination of H_2O_2 and $O_2^{\bullet-}$ is essential for antioxidant defense in cellular or dietary systems. By donating electrons to H_2O_2, a robust antioxidant might neutralize it into water.[59] Therefore, as efficient antioxidants, different nanoparticles have been investigated. Here antioxidant properties of ZnO NPs were evaluated using the above-discussed method. Percent of H_2O_2 scavenging activity of ZnO NPs and ascorbic acid is presented in Table 3. When compared to ascorbic acid, no significant difference was found in the radical scavenging activity of ZnO NPs, which signifies that the antioxidant effect of ZnO NPs was comparable to that of standard ascorbic acid.

3.8.3. Percent ABTS Radical Scavenging Activity. ABTS assay evaluated the capacity of antioxidants to scavenge the stable radical cation 2,2′-azinobis (3-ethylbenzothiazoline-6-sulfonic acid (ABTS$\bullet^+$). In this assay, (ABTS$\bullet^+$) is produced by a strong oxidant such as peroxide and persulfate mediated conversion of ABTS. Strong antioxidants act either by donating electrons and the radical or by donating hydrogen atoms which scavenges the radical. During this mechanism, in the presence of antioxidants, a blue-green chromophore with maximum absorption at 734 nm is produced, and hence, it is selected as the optimum wavelength by investigators.[60] The results obtained by using ZnO NPs and ascorbic acid as antioxidants are presented in Table 4, and the percent ABTS scavenging activity of ZnO NPs was comparable to that of ascorbic acid as no significant difference was observed between them, which signifies that the antioxidant effect of plant extract ZnO NPs was comparable to that of standard ascorbic acid.

3.8.4. Stability of As-Prepared Aerva persica-Mediated ZnO NPs. The stability and reusability of as-synthesized *Aerva persica*-mediated ZnO NPs were examined by performing

Table 2. Percent DPPH Scavenging Activity of Ascorbic Acid, and ZnO NPs at Various Concentrations[a]

		DPPH radical scavenging activity		
s. no	drugs	100 μg/mL	250 μg/mL	500 μg/mL
1	ascorbic acid	67.54 ± 0.64	75.34 ± 5.81	91.563 ± 1.60
2	ZnO NPs	54.30 ± 0.46$^{1\alpha}$	91.56 ± 1.603$^{ns\alpha}$	84.07 ± 0.94$^{ns\alpha}$

[a]Data are expressed as mean ± SEM; analysis was done using GraphPad Prism version 9, where data are analyzed using one-way ANOVA followed by Dunnett's test of multiple comparisons. Criteria of statistical significance was $p < 0.05$. $^1p < 0.000$; ns denotes not significant ($n = 3$); $^{\alpha}$comparison to ascorbic acid.

https://doi.org/10.1021/acsomega.3c08143
ACS Omega 2024, 9, 15882−15892

Table 3. Percent H_2O_2 Scavenging Activity of Ascorbic Acid, and ZnO NPs atVarious Concentrations[a]

s. no.	drugs	percent H_2O_2 scavenging activity		
		100 μg/mL	250 μg/mL	500 μg/mL
1	ascorbic acid	63.42 ± 1.74	76.47 ± 1.26	85.32 ± 1.69
2	ZnO NPs	64. 56 ± 1.20$^{ns\alpha}$	80.25 ± 1.90$^{ns\alpha}$	81.39 ± 2.12$^{ns\alpha}$

[a]Data are expressed as mean ± SEM. Analysis was done using GraphPad Prism version 9, where data are analyzed using one-way ANOVA followed by Dunnett's test of multiple comparisons. Criteria of statistical significance was $p < 0.05$. ns denotes not significant ($n = 3$).

Table 4. Percent ABTS Radical Scavenging Activity of Ascorbic Acid, and ZnO NPs at Various Concentrations[a]

s. no.	drug	ABTS radical scavenging activity		
		100 μg/mL	250 μg/mL	500 μg/mL
1	ascorbic acid	55.97 ± 4.32	86.35 ± 1.94	79.91 ± 1.05
2	ZnO NPs	56.40 ± 2.31$^{ns\alpha}$	87.82 ± 3.00$^{ns\alpha}$	84.15 ± 1.89$^{ns\alpha}$

[a]The data are presented as a mean ± SEM. The analysis was performed in GraphPad Prism version 9, with one-way ANOVA and Dunnett's test for multiple comparisons used to examine the data. Criteria of statistical significance was $p < 0.05$. ns denotes not significant ($n = 3$).

DPPH-free radical scavenging activity of recovered nanoparticles by using the above-mentioned approach. To perform the stability test, the reaction mixture after analyzing the scavenging activity was centrifuged to recover the nanoparticles, then washed, dried in the oven, and reused for the next cycle of DPPH radical scavenging activity. Figure 9

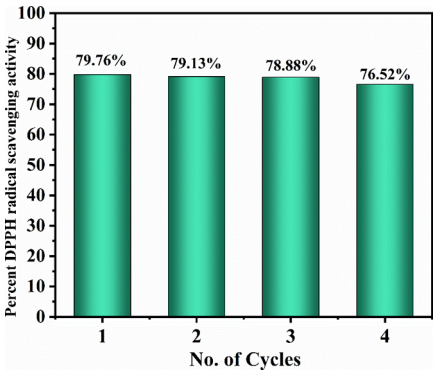

Figure 9. Stability and reusability of as-synthesized *Aerva persica*-mediated ZnO NPs

displays the stability and reusability of as-synthesized ZnO NPs up to four consecutive cycles. From the results, it was observed that no significant changes were observed in antioxidant activity after four cycles of reaction batches, which confirmed the stability of as-prepared ZnO NPs.

3.8.5. In Vivo Anti-Inflammatory Activity. 3.8.5.1. Inhibition of Carrageenan-Induced Paw Edema. The carrageenan-induced paw edema model is commonly applied to estimate the anti-inflammatory effects of natural and synthesized compounds. Carrageenan is an antigen-free physiological agent with no discernible systemic effects. Carrageenan's stimulation of phospholipase A2 begins the early phase of inflammation, whereas cytotoxic actions promote the progression of inflammation. Carrageenan model is often associated with cyclooxygenase pathway activation. In this preclinical model, glucocorticoids and prostaglandin antagonists demonstrate anti-inflammatory action. Carrageenan-induced edema is illustrated as a biphasic curve. The initial phase of inflammation caused by carrageenan is partially attributed to injection trauma and the release of acute mediators including serotonin and histamine. Prostaglandins are the primary mediators of the second phase of carrageenan-induced inflammation, which begins around 3 h after carrageenan administration.[61]

Injection of carrageenan-induced edema in rat paw and an efficient anti-inflammatory drug will be able to reduce the carrageenan-induced edema, which was measured by volume displacement of mercury by the edematous paw. Table 5 presents volume displacement and percent inhibition of inflammation by indomethacin and ZnO NPs. At 0 h, the difference in volume displacement of mercury by rat paw of indomethacin-treated and ZnO NP-treated rats compared to the negative control rat was found to be insignificant. After 1 and 2 h of the drug administration, a significant reduction in the mercury volume was found in indomethacin-0 and ZnO NP-treated group ($p < 0.0001$. The difference in volume displacement of mercury between indomethacin and ZnO NPs was found to be insignificant which signifies that the potency of the ZnO NPs in reduction of inflammation was found to be equivalent to that of standard indomethacin. Also, the percent inhibition of inflammation by ZnO NPs was found to be 78.57 and 79.76% at 1 and 2 h respectively, which was found to be very close to that of indomethacin which is 79.76 and 80.95% at 1 and 2 h. Therefore, from this investigation, it was observed that ZnO NPs were effectively able to combat carrageenan-induced paw edema and are depicted to be a potent anti-inflammatory agent.

Table 5. Volume Displacement of Mercury by Rat Paw in the Carrageenan-Induced Paw Edema Model of Inflammation[a]

s. no.	treatment groups	volume displacement of mercury (mL)			percent inhibition of edema	
		0 h	1 h	2 h	1 h	2 h
1	negative control	0.82 ± 0.03	0.85 ± 0.03	0.86 ± 0.025	−3.65	−4.87
2	indomethacin (50 mg/kg)	0.84 ± 0.03$^{ns\alpha}$	0.17 ± 0.016$^{1\alpha}$	0.16 ± 0.02$^{1\alpha}$	79.76	80.95
3	ZnO NPs (36.5 mg/kg)	0.84 ± 0.03$^{ns\alpha\beta}$	0.18 ± 0.017$^{1\alpha ns\beta}$	0.17 ± 0.011$^{1\alpha ns\beta}$	78.57	79.76

[a]The data are presented as a mean ± SEM. The analysis was performed in GraphPad Prism version 9, with one-way ANOVA and Dunnett's test for multiple comparisons used to examine the data. Criteria of statistical significance was $p < 0.05$. $^1p < 0.0001$, ns denotes not significant ($n = 6$). $^{\alpha}$Comparison to negative control; $^{\beta}$comparison to indomethacin.

https://doi.org/10.1021/acsomega.3c08143
ACS Omega 2024, 9, 15882−15892

Table 6. Comparative Table of Antioxidant Activity and Anti-inflammatory Activity of ZnO with the Reported Data

s. no.	metal oxide	activity	concentration	percent scavenging activity	ref
1	FeONPs	antioxidant	1000 μg/mL	81.5%	62
2	ZnO@OFE NPs	antioxidant	200 μg/mL	75%	63
3	ZnO NPs *Curcuma longa*	antioxidant	200 μg/mL	70%	64
4	ZnO NPs *Polygala tenuifolia* root extract	antioxidant	1 mg/mL	45.47%	65
5	*Camellia sinensis* extract CSE-CuO NPs	antioxidant	250 μg/mL	28.8%	66
6	*Prunus africana* bark extract PAE-CuO NPs	antioxidant	250 μg/mL	28.5%	
7	CuO-NP	anti-inflammatory	400 mg/mL	74% in 48 h	67
8	*Senecio chrysanthemoides* leaf extract mediated ZnO NPs	anti-inflammatory	100 μg/mL	73%	68
9	*Aerva Persica*-mediated ZnO NPs	antioxidant	250 μg/mL	91%	this work
10	*Aerva Persica*-mediated ZnO NPs	anti-inflammatory	36.5 mg/mL	79.76% in 2 h	this work

The antioxidant and anti-inflammatory activity of as-prepared ZnO nanoparticles was compared with the already reported activity of different plant extract-mediated metal oxides, which is tabulated in Table 6.

4. CONCLUSIONS

Aerva persica root extract-mediated ZnO nanoparticles were synthesized successfully through a simple, green, and facile route. The powder X-ray diffraction confirms the monocrystalline nature and high crystallinity of as-synthesized ZnO nanoparticles with an average crystallite size of 23.8 nm. The band gap was estimated using UV-DRS studies and calculated using the Kubelka−Munk equation, which is found to be 3.18 eV. Furthermore, the morphological analysis was done with FESEM and TEM studies in which the high-resolution FESEM micrograph shows flakes-like particles overlapping which results in the growth of nanoparticles. The average particle size was calculated from the TEM micrograph which was found to be ∼45 nm. The surface area of as-synthesized ZnO nanoparticles was also evaluated by using BET surface area studies, which is estimated as 43 m^2/g. In vitro antioxidant activities revealed that ZnO NPs exhibited strong DPPH radical, H_2O_2 radical, and ABTS radical scavenging activity with potency comparable to that of the standard. Similarly, the in vivo anti-inflammatory model revealed that ZnO NPs showed a significant reduction of carrageenan induced paw edema in experimental rats. Therefore, it has been concluded that ZnO NPs show significant antioxidant and anti-inflammatory activity, which is comparable to standard samples and can be further explored for different biomedical applications. In addition, more research is needed to explore the mode of action to understand the mechanism involved in these applications. In the future, this study can be further used as a basis to explore the mechanism involved in the antioxidant and anti-inflammatory action of different metal oxides.

AUTHOR INFORMATION

Corresponding Author

Umar Farooq − *Chemistry Department, School of Basic Sciences, Galgotias University, Greater Noida 201309, India;* orcid.org/0000-0001-8068-7962; Phone: +91-9682565419; Email: darumer27@gmail.com

Authors

Kaneez Fatima − *Faculty of Pharmacy, Maulana Azad University, Jodhpur 342802 Rajasthan, India; INTI International University, 71800 Nilai, Negeri Sembilan, Malaysia*

Mohammad Asif − *Faculty of Pharmacy, Lachoo Memorial College of Science and Technology, Jodhpur 342001 Rajasthan, India*

Sadaf Jamal Gilani − *Department of Basic Health Sciences, Foundation Year, Princess Nourah bint Abdulrahman University, Riyadh 11671, Saudi Arabia;* orcid.org/0000-0002-9590-3856

May Nasser Bin Jumah − *Saudi Society for Applied Science, Environment and Biomaterial Unit, Health Sciences Research Center, and Biology Department, College of Science, Princess Nourah bint Abdulrahman University, Riyadh 11671, Saudi Arabia*

Mohammed Muqtader Ahmed − *Department of Pharmaceutics, College of Pharmacy, Prince Sattam Bin Abdulaziz University, Al-Kharj 11942, Saudi Arabia*

Complete contact information is available at: https://pubs.acs.org/10.1021/acsomega.3c08143

Author Contributions

Methodology and Resources, K.F. and M.A.; Software and Formal analysis, U.F.; .Investigation, K.F., M.A. and U.F.; Writing − original draft and Funding acquisition, S.J.G.; Writing − review and editing, M.N.B.J. and M.M.A.

Funding

This research project was funded by Princess Nourah bint Abdulrahman University Researchers Supporting Project number (PNURSP2023R108), Princess Nourah bint Abdulrahman University, Riyadh, Saudi Arabia.

Notes

The authors declare no competing financial interest.

ACKNOWLEDGMENTS

Author K.F., M.A. are highly thankful to Maulana Azad University and Lachoo Memorial College of Science and Technology for providing space and facilities to carry out their research activities, Author U.F. is grateful to the Department of Chemistry, School of Basic Sciences, Galgotias University to provide basic research facilities for his research activities. This research was supported by Princess Nourah bint Abdul Rahman University Researchers Supporting Project number (PNURSP2023R108), Princess Nourah bint Abdulrahman University, Riyadh, Saudi Arabia.

REFERENCES

(1) Khan, I.; Saeed, K.; Khan, I. Nanoparticles: Properties, applications and toxicities. *Arabian journal of chemistry* **2019**, *12* (7), 908−931.

(2) Harish, V.; Tewari, D.; Gaur, M.; Yadav, A. B.; Swaroop, S.; Bechelany, M.; Barhoum, A. Review on nanoparticles and nano-

https://doi.org/10.1021/acsomega.3c08143
ACS Omega 2024, 9, 15882−15892

structured materials: Bioimaging, biosensing, drug delivery, tissue engineering, antimicrobial, and agro-food applications. *Nanomaterials* **2022**, *12* (3), 457.
(3) Bhardwaj, B.; Singh, P.; Kumar, A.; Kumar, S.; Budhwar, V. Eco-friendly greener synthesis of nanoparticles. *Advanced Pharmaceutical Bulletin* **2020**, *10* (4), 566.
(4) Farooq, U.; Phul, R.; Alshehri, S. M.; Ahmed, J.; Ahmad, T. Electrocatalytic and enhanced photocatalytic applications of sodium niobate nanoparticles developed by citrate precursor route. *Sci. Rep.* **2019**, *9* (1), 4488.
(5) Farooq, U.; Chaudhary, P.; Ingole, P. P.; Kalam, A.; Ahmad, T. Development of cuboidal KNbO3@ α-Fe2O3 hybrid nanostructures for improved photocatalytic and photoelectrocatalytic applications. *Acs Omega* **2020**, *5* (32), 20491−20505.
(6) Phul, R.; Kaur, C.; Farooq, U.; Ahmad, T. Ascorbic acid assisted synthesis, characterization, and catalytic application of copper nanoparticles. *Mater. Sci. Eng. Int. J.* **2018**, *2*, 90−94.
(7) Naaz, F.; Farooq, U.; Khan, M. M.; Ahmad, T. Multifunctional efficacy of environmentally benign silver nanospheres for organic transformation, photocatalysis, and water remediation. *ACS omega* **2020**, *5* (40), 26063−26076.
(8) Farooq, U.; Ahmad, T.; Naaz, F.; Islam, S. U. Review on metals and metal oxides in sustainable energy production: progress and perspectives. *Energy & Fuels* **2023**, *37* (3), 1577−1632.
(9) Dhandapani, K. V.; Anbumani, D.; Gandhi, A. D.; Annamalai, P.; Muthuvenkatachalam, B. S.; Kavitha, P.; Ranganathan, B. Green route for the synthesis of zinc oxide nanoparticles from Melia azedarach leaf extract and evaluation of their antioxidant and antibacterial activities. *Biocatalysis and Agricultural Biotechnology* **2020**, *24*, No. 101517.
(10) Singh, R.; Hano, C.; Nath, G.; Sharma, B. Green biosynthesis of silver nanoparticles using leaf extract of Carissa carandas L. and their antioxidant and antimicrobial activity against human pathogenic bacteria. *Biomolecules* **2021**, *11* (2), 299.
(11) Wu, S.; Rajeshkumar, S.; Madasamy, M.; Mahendran, V. Green synthesis of copper nanoparticles using Cissus vitiginea and its antioxidant and antibacterial activity against urinary tract infection pathogens. *Artificial Cells, Nanomedicine, and Biotechnology* **2020**, *48* (1), 1153−1158.
(12) Joshi, C. G.; Danagoudar, A.; Poyya, J.; Kudva, A. K.; Dhananjaya, B. L. Biogenic synthesis of gold nanoparticles by marine endophytic fungus-Cladosporium cladosporioides isolated from seaweed and evaluation of their antioxidant and antimicrobial properties. *Process Biochem.* **2017**, *63*, 137−144.
(13) Rana, A.; Pathak, S.; Lim, D. K.; Kim, S. K.; Srivastava, R.; Sharma, S. N.; Verma, R. Recent Advancements in Plant-and Microbe-Mediated Synthesis of Metal and Metal Oxide Nanomaterials and Their Emerging Antimicrobial Applications. *ACS Applied Nano Materials* **2023**, *6* (10), 8106−8134.
(14) Mishra, P. M. Plant-Mediated Synthesis of Metal Oxide Nanocomposites for Environmental Remediation. *Green Nanoparticles: Synthesis and Biomedical Applications* **2020**, 359−369.
(15) Bachheti, R. K.; Godebo, Y.; Bachheti, A.; Yassin, M. O.; Husen, A. Root-based fabrication of metal/metal-oxide nanomaterials and their various applications. *Nanomaterials for Agriculture and Forestry Applications* **2020**, 135−166.
(16) Raha, S.; Ahmaruzzaman, M. ZnO nanostructured materials and their potential applications: progress, challenges and perspectives. *Nanoscale Advances* **2022**, *4* (8), 1868−1925.
(17) Anjum, S.; Hashim, M.; Malik, S. A.; Khan, M.; Lorenzo, J. M.; Abbasi, B. H.; Hano, C. Recent advances in zinc oxide nanoparticles (ZnO NPs) for cancer diagnosis, target drug delivery, and treatment. *Cancers* **2021**, *13* (18), 4570.
(18) Mirzaei, H.; Darroudi, M. Zinc oxide nanoparticles: Biological synthesis and biomedical applications. *Ceram. Int.* **2017**, *43* (1), 907−914.
(19) Jiang, J.; Pi, J.; Cai, J. The advancing of zinc oxide nanoparticles for biomedical applications. *Bioinorg. Chem. Appl.* **2018**, *2018*, No. 1062562, DOI: 10.1155/2018/1062562.
(20) Zhang, H. J.; Xiong, H. M. Biological applications of ZnO nanoparticles. *Current Molecular Imaging (Discontinued)* **2013**, *2* (2), 177−192.
(21) Mishra, P. K.; Mishra, H.; Ekielski, A.; Talegaonkar, S.; Vaidya, B. Zinc oxide nanoparticles: a promising nanomaterial for biomedical applications. *Drug discovery today* **2017**, *22* (12), 1825−1834.
(22) Zhang, Z. Y.; Xiong, H. M. Photoluminescent ZnO nanoparticles and their biological applications. *Materials* **2015**, *8* (6), 3101−3127.
(23) Kim, S.; Lee, S. Y.; Cho, H. J. Doxorubicin-wrapped zinc oxide nanoclusters for the therapy of colorectal adenocarcinoma. *Nanomaterials* **2017**, *7* (11), 354.
(24) Xiong, H. M. ZnO nanoparticles applied to bioimaging and drug delivery. *Adv. Mater.* **2013**, *25* (37), 5329−5335.
(25) Vijayakumar, S.; Vaseeharan, B.; Malaikozhundan, B.; Shobiya, M. Laurus nobilis leaf extract mediated green synthesis of ZnO nanoparticles: Characterization and biomedical applications. *Biomedicine & Pharmacotherapy* **2016**, *84*, 1213−1222.
(26) Nagajyothi, P. C.; Cha, S. J.; Yang, I. J.; Sreekanth, T. V. M.; Kim, K. J.; Shin, H. M. Antioxidant and anti-inflammatory activities of zinc oxide nanoparticles synthesized using Polygala tenuifolia root extract. *Journal of Photochemistry and Photobiology B: Biology* **2015**, *146*, 10−17.
(27) Rajakumar, G.; Thiruvengadam, M.; Mydhili, G.; Gomathi, T.; Chung, I. M. Green approach for synthesis of zinc oxide nanoparticles from Andrographis paniculata leaf extract and evaluation of their antioxidant, anti-diabetic, and anti-inflammatory activities. *Bioprocess and biosystems engineering* **2018**, *41*, 21−30.
(28) Velsankar, K.; Venkatesan, A.; Muthumari, P.; Suganya, S.; Mohandoss, S.; Sudhahar, S. Green inspired synthesis of ZnO nanoparticles and its characterizations with biofilm, antioxidant, anti-inflammatory, and anti-diabetic activities. *J. Mol. Struct.* **2022**, *1255*, No. 132420.
(29) Mutukwa, D.; Taziwa, R.; Khotseng, L. E. A review of the green synthesis of ZnO nanoparticles utilising Southern African indigenous medicinal plants. *Nanomaterials* **2022**, *12* (19), 3456.
(30) Pham-Huy, L. A.; He, H.; Pham-Huy, C. Free radicals, antioxidants in disease and health. *Int. J. Biomed. Sci.* **2008**, *4* (2), 89.
(31) Bitto, A.; Pizzino, G.; Irrera, N.; Cucinotta, M.; Pallio, G.; Mannino, F.; Arcoraci, V. Oxidative stress: harms and benefits for human health. *Oxid. Med. Cell. Longevity* **2017**, *2017*, No. 8416763, DOI: 10.1155/2017/8416763.
(32) Chen, L.; Deng, H.; Cui, H.; Fang, J.; Zuo, Z.; Deng, J.; Zhao, L. Inflammatory responses and inflammation-associated diseases in organs. *Oncotarget* **2018**, *9* (6), 7204.
(33) Arango Duque, G.; Descoteaux, A. Macrophage cytokines: involvement in immunity and infectious diseases. *Front. Immunol.* **2014**, *5*, 491.
(34) Ahmad, R.; Amin, F.; Khattak, B.; Alotaibi, A.; Qasim, M.; Ahmad, I.; Ullah, R. Green synthesis of copper oxide nanoparticles using Aerva javanica leaf extract and their characterization and investigation of in vitro antimicrobial potential and cytotoxic activities. *J. Evidence-Based Complementary Altern. Med.* **2021**, *2021*, No. 5589703, DOI: 10.1155/2021/5589703.
(35) Dawood, S.; Afzal, G.; Jamal, A.; Kiran, S.; Mustafa, G.; Ahmad, F.; Saeed, S. AERVA JAVANICA MEDIATED SYNTHESIS, CHARACTERIZATION AND ANTIMICROBIAL EVALUATION OF ZINC OXIDE NANOPARTICLES. *J. Anim. Plant Sci.* **2022**, *32* (2), 547 DOI: 10.36899/JAPS.2022.2.0453.
(36) Priya, D. D.; Nandhakumar, M.; Shanavas, S.; Arasu, M. V.; Al-Dhabi, N. A.; Madhumitha, G. Aerva lanata-mediated bio-treated production of copper oxide nanoparticles, optimization by BBD−RSM method and it behaviour against water related mosquito. *Applied Nanoscience* **2021**, *11*, 207−216.
(37) Bala, N.; Saha, S.; Chakraborty, M.; Maiti, M.; Das, S.; Basu, R.; Nandy, P. Green synthesis of zinc oxide nanoparticles using Hibiscus subdariffa leaf extract: effect of temperature on synthesis, anti-bacterial activity and anti-diabetic activity. *RSC Advances* **2015**, *5* (7), 4993−5003.

https://doi.org/10.1021/acsomega.3c08143
ACS Omega 2024, 9, 15882−15892

(38) Jayakar, V.; Lokapur, V.; Nityasree, B. R.; Chalannavar, R. K.; Lasrado, L. D.; Shantaram, M. Optimization and green synthesis of zinc oxide nanoparticle using Garcinia cambogia leaf and evaluation of their antioxidant and anticancer property in kidney cancer (A498) cell lines. *Biomedicine* **2021**, *41* (2), 206−222.
(39) Sivasankarapillai, V. S.; Krishnamoorthy, N.; Eldesoky, G. E.; Wabaidur, S. M.; Islam, M. A.; Dhanusuraman, R.; Ponnusamy, V. K. One-pot green synthesis of ZnO nanoparticles using Scoparia Dulcis plant extract for antimicrobial and antioxidant activities. *Applied Nanoscience* **2023**, *13* (9), 6093−6103.
(40) Safawo, T.; Sandeep, B. V.; Pola, S.; Tadesse, A. Synthesis and characterization of zinc oxide nanoparticles using tuber extract of anchote (Coccinia abyssinica (Lam.) Cong.) for antimicrobial and antioxidant activity assessment. *OpenNano* **2018**, *3*, 56−63.
(41) Alsareii, S. A.; Manaa Alamri, A.; AlAsmari, M. Y.; Bawahab, M. A.; Mahnashi, M. H.; Shaikh, I. A.; Kumbar, V. Synthesis and characterization of silver nanoparticles from Rhizophora apiculata and studies on their wound healing, antioxidant, anti-inflammatory, and cytotoxic activity. *Molecules* **2022**, *27* (19), 6306.
(42) González-Palma, I.; Escalona-Buendía, H. B.; Ponce-Alquicira, E.; Téllez-Téllez, M.; Gupta, V. K.; Díaz-Godínez, G.; Soriano-Santos, J. Evaluation of the antioxidant activity of aqueous and methanol extracts of Pleurotus ostreatus in different growth stages. *Front. Microbiol.* **2016**, *7*, 1099.
(43) Kedi, P. B. E.; Meva, F. E. A.; Kotsedi, L.; Nguemfo, E. L.; Zangueu, C. B.; Ntoumba, A. A.; Maaza, M. Eco-friendly synthesis, characterization, in vitro and in vivo anti-inflammatory activity of silver nanoparticle-mediated Selaginella myosurus aqueous extract. *Int. J. Nanomed.* **2018**, *13*, 8537−8548.
(44) Bidian, C.; Filip, G. A.; David, L.; Moldovan, B.; Baldea, I.; Olteanu, D.; Clichici, S. Viburnum opulus fruit extract-capped gold nanoparticles attenuated oxidative stress and acute inflammation in carrageenan-induced paw edema model. *Green Chem. Lett. Rev.* **2022**, *15* (2), 320−336.
(45) Basak, M.; Rahman, M. L.; Ahmed, M. F.; Biswas, B.; Sharmin, N. The use of X-ray diffraction peak profile analysis to determine the structural parameters of cobalt ferrite nanoparticles using Debye-Scherrer, Williamson-Hall, Halder-Wagner and Size-strain plot: Different precipitating agent approach. *J. Alloys Compd.* **2022**, *895*, No. 162694.
(46) Talam, S.; Karumuri, S. R.; Gunnam, N. Synthesis, characterization, and spectroscopic properties of ZnO nanoparticles. *Int. Scholarly Res. Not.* **2012**, *2012*, No. 372505, DOI: 10.5402/2012/372505.
(47) Kohan, M. G.; You, S.; Camellini, A.; Concina, I.; Rossi, M. Z.; Vomiero, A. Optical field coupling in ZnO nanorods decorated with silver plasmonic nanoparticles. *J. Mater. Chem. C* **2021**, *9* (43), 15452−15462.
(48) Mashentseva, A. A.; Aimanova, N. A.; Parmanbek, N.; Temirgaziyev, B. S.; Barsbay, M.; Zdorovets, M. V. Serratula coronata L. mediated synthesis of ZnO nanoparticles and their application for the removal of alizarin yellow R by photocatalytic degradation and adsorption. *Nanomaterials* **2022**, *12* (19), 3293.
(49) Nimbalkar, A. R.; Patil, M. G. Synthesis of ZnO thin film by sol-gel spin coating technique for H2S gas sensing application. *Physica B: Condensed Matter* **2017**, *527*, 7−15.
(50) Kumar, G. S.; Rajendran, S.; Karthi, S.; Govindan, R.; Girija, E. K.; Karunakaran, G.; Kuznetsov, D. Green synthesis and antibacterial activity of hydroxyapatite nanorods for orthopedic applications. *MRS communications* **2017**, *7* (2), 183−188.
(51) Zheng, Y.; Fu, L.; Han, F.; Wang, A.; Cai, W.; Yu, J.; Peng, F. Green biosynthesis and characterization of zinc oxide nanoparticles using Corymbia citriodora leaf extract and their photocatalytic activity. *Green Chem. Lett. Rev.* **2015**, *8* (2), 59−63.
(52) Anbuvannan, M.; Ramesh, M.; Viruthagiri, G.; Shanmugam, N.; Kannadasan, N. Synthesis, characterization and photocatalytic activity of ZnO nanoparticles prepared by biological method. *Spectrochimica Acta Part A: Molecular and Biomolecular Spectroscopy* **2015**, *143*, 304−308.
(53) Priya, D. D.; Nandhakumar, M.; Shanavas, S.; Arasu, M. V.; Al-Dhabi, N. A.; Madhumitha, G. Aerva lanata-mediated bio-treated production of copper oxide nanoparticles, optimization by BBD−RSM method and it behaviour against water related mosquito. *Applied Nanoscience* **2021**, *11*, 207−216.
(54) Benhebal, H.; Chaib, M.; Salmon, T.; Geens, J.; Leonard, A.; Lambert, S. D.; Heinrichs, B. Photocatalytic degradation of phenol and benzoic acid using zinc oxide powders prepared by the sol−gel process. *Alexandria Eng. J.* **2013**, *52* (3), 517−523.
(55) Sabura Begum, P. M.; Mohammed Yusuff, K. K.; Joseph, R. Preparation and use of nano zinc oxide in neoprene rubber. *Int. J. Polym. Mater.* **2008**, *57* (12), 1083−1094.
(56) Naseer, M.; Aslam, U.; Khalid, B.; Chen, B. Green route to synthesize Zinc Oxide Nanoparticles using leaf extracts of Cassia fistula and Melia azadarach and their antibacterial potential. *Sci. Rep.* **2020**, *10* (1), 9055.
(57) Rahman, M. M.; Islam, M. B.; Biswas, M.; Khurshid Alam, A. H. M. In vitro antioxidant and free radical scavenging activity of different parts of Tabebuia pallida growing in Bangladesh. *BMC Res. Notes* **2015**, *8* (1), 621.
(58) Hazra, B.; Biswas, S.; Mandal, N. Antioxidant and free radical scavenging activity of Spondias pinnata. *BMC Complementary Altern. Med.* **2008**, *8* (1), 63.
(59) Mukhopadhyay, D.; Dasgupta, P.; Roy, D. S.; Palchoudhuri, S.; Chatterjee, I.; Ali, S.; Dastidar, S. G. A sensitive in vitro spectrophotometric hydrogen peroxide scavenging assay using 1, 10-phenanthroline. *Free Radicals Antioxid.* **2016**, *6* (1), 124−132.
(60) AsokKumar, K.; UmaMaheswari, M.; Sivashanmugam, A. T.; SubhadraDevi, V.; Subhashini, N.; Ravi, T. K. Free radical scavenging and antioxidant activities of Glinus oppositifolius (carpet weed) using different in vitro assay systems. *Pharmaceutical Biology* **2009**, *47* (6), 474−482.
(61) Patil, K. R.; Mahajan, U. B.; Unger, B. S.; Goyal, S. N.; Belemkar, S.; Surana, S. J.; Patil, C. R. Animal models of inflammation for screening of anti-inflammatory drugs: implications for the discovery and development of phytopharmaceuticals. *Int. J. Mol. Sci.* **2019**, *20* (18), 4367.
(62) Shabbir, M. A.; Naveed, M.; Rehman, S. U.; Ain, N. U.; Aziz, T.; Alharbi, M.; Alasmari, A. F. Synthesis of iron oxide nanoparticles from Madhuca indica plant extract and assessment of their cytotoxic, antioxidant, anti-inflammatory, and anti-diabetic properties via different nanoinformatics approaches. *ACS omega* **2023**, *8* (37), 33358−33366.
(63) Ghaffar, S.; Abbas, A.; Naeem-ul-Hassan, M.; Assad, N.; Sher, M.; Ullah, S.; Amin, H. M. Improved Photocatalytic and Antioxidant Activity of Olive Fruit Extract-Mediated ZnO Nanoparticles. *Antioxidants* **2023**, *12* (6), 1201.
(64) Jacob, V.; P, R. In vitro analysis: The antimicrobial and antioxidant activity of zinc oxide nanoparticles from Curcuma longa. *Asian J. Pharm. Clin. Res.* **2019**, *12* (1), 200 DOI: 10.22159/ajpcr.2019.v12i1.28808.
(65) Nagajyothi, P. C.; Cha, S. J.; Yang, I. J.; Sreekanth, T. V. M.; Kim, K. J.; Shin, H. M. Antioxidant and anti-inflammatory activities of zinc oxide nanoparticles synthesized using Polygala tenuifolia root extract. *Journal of Photochemistry and Photobiology B: Biology* **2015**, *146*, 10−17.
(66) Ssekatawa, K.; Byarugaba, D. K.; Angwe, M. K.; Wampande, E. M.; Ejobi, F.; Nxumalo, E.; Kirabira, J. B. Phyto-mediated copper oxide nanoparticles for antibacterial, antioxidant and photocatalytic performances. *Front. Bioeng. Biotechnol.* **2022**, *10*, No. 820218.
(67) Faisal, S.; Jan, H.; Abdullah Alam, I.; Rizwan, M.; Hussain, Z.; Uddin, M. N. In vivo analgesic, anti-inflammatory, and anti-diabetic screening of Bacopa monnieri-synthesized copper oxide nanoparticles. *ACS Omega* **2022**, *7* (5), 4071−4082.
(68) Khan, W.; Zahoor, S.; Sheraz, S.; Shams, D. F.; Rehman, G.; Nayab, S.; Shah, M. I. A. Biosynthesis and Anti-inflammatory Activity of Zinc Oxide Nanoparticles Using Leaf Extract of Senecio chrysanthemoides. *BioMed Res. Int.* **2023**, *2023*, No. 3280708, DOI: 10.1155/2023/3280708.

https://doi.org/10.1021/acsomega.3c08143
ACS Omega 2024, 9, 15882−15892